Sliding Clamp of the Bacteriophage T4 Polymerase Has Open and Closed Subunit Interfaces in Solution†

Stephen C. Alley, Vincent K. Shier, Ernesto Abel-Santos, Daniel J. Sexton,‡ Patrice Soumillion,§ and Stephen J. Benkovic*

Department of Chemistry, 152 Davey Laboratory, The Pennsylvania State University, University Park, Pennsylvania 16802

Received November 25, 1998; Revised Manuscript Received April 23, 1999

ABSTRACT: The sliding clamps of bacteriophage T4 (gp45), *Escherichia coli* (β clamp), and yeast (PCNA) are required for processive DNA synthesis by their cognate DNA polymerases. The X-ray crystal structures of all three of these clamps have been shown to be closed, circular complexes. This paper reports investigations of the solution structure of bacteriophage T4 gp45 by analytical ultracentrifugation, fluorescence, and hydrodynamic modeling. Mutants of gp45 with inter- and intrasubunit disulfide bonds were created to alter the solution structure of gp45, with additional mutagenesis used to investigate the importance of the proline-rich loop region found between the two domains of each gp45 monomer. The wild-type gp45 trimer assembles from monomers cooperatively with a dissociation constant of 0.21 μM^2 and values between 0.088 and 0.32 μM^2 for the mutants. Velocity ultracentrifugation experiments showed that wild-type gp45 possesses a sedimentation coefficient strongly dependent on concentration, typical of asymmetric or elongated molecules, that when extrapolated to zero concentration yields a sedimentation coefficient of 4.0 S. The loop and the disulfide mutants exhibited sedimentation coefficients with little concentration dependence, typical of symmetric or spherical molecules, that when extrapolated to zero concentration yielded sedimentation coefficients of 4.4−4.8 S. The lower sedimentation coefficient in the former case is consistent with wild-type gp45 being more asymmetric or elongated than the mutant forms. Fluorescence-resonance energy-transfer experiments were used to measure the distance between two amino acids (W91 and V162C-coumarin) on opposite sides of the gp45 subunit interface. For an intrasubunit disulfide mutant, the distance between these two amino acids was determined to be 19 Å (14 Å in the X-ray crystal structure), consistent with a closed complex. For the mutants without intrasubunit disulfides, the efficiency of fluorescence-resonance energy transfer was in accord with a model of gp45 being an open complex composed of two closed subunit interfaces and a third open interface separated by a distance of 35−38 Å. The collective data supplemented with hydrodynamic modeling were consistent with gp45 subunit separation achieved within the plane of the gp45 ring.

DNA replication in many viruses, prokaryotes, and eukaryotes exhibits striking similarities. For example, the structures of the sliding clamps from bacteriophage T4 (J. Kuriyan, personal communication), *Escherichia coli* (*1*), and yeast (*2*) have all been shown to be mutimeric closed circular complexes by X-ray crystallography. Newly synthesized DNA presumably travels through the centers of these closed circles and thereby forms topological links between the DNA polymerases and the DNA, causing significant increases in processivity. All three of these organisms likewise possess clamp loading proteins that load these clamps onto DNA by mechanisms that are not completely understood (reviewed in refs *3* and *4*). Specifically, processive leading-strand DNA synthesis in bacteriophage T4 requires four proteins to generate the holoenzyme complex: the DNA polymerase (gp43), the trimeric sliding clamp (gp45), and a clamp loader (a 4:1 complex of gp44 and gp62). The clamp loader, however, is a transient component and acts catalytically to load the clamp protein onto the DNA primer-template and chaperone the polymerase onto the gp45−DNA complex (*5*).

Detailed structural information for some of the individual holoenzyme components has been obtained by X-ray crystallography, while lower-resolution experiments have probed the structure of the holoenzyme. In addition to the X-ray crystal structure of gp45, the structure of the DNA polymerase from bacteriophage RB69 [63% identity with gp43 from T4 (*6*)] is known (*7*). These two structures permit more detailed mechanistic questions regarding holoenzyme assembly, DNA synthesis, and holoenzyme disassembly to be addressed. Previous investigations have employed fluorescence spectroscopy and photo-cross-linking to probe protein−protein interactions during and following holoenzyme assembly by incorporating site-specific labels into the trimeric gp45. Wild-type gp45 contains no cysteine residues, so mutagenesis can be used to incorporate unique thiols at any location within each gp45 monomer. These studies have

† This work was supported by National Institutes of Health Grants GM13306 (S.J.B.) and GM19492 (S.C.A.).

* To whom correspondence should be addressed. E-mail: sjb1@psu.edu. Phone: (814) 865-2882. Fax: (814) 865-2973.

‡ Current address: Dyax Corporation, One Kendall Square, Building 600, 5th Floor, Cambridge, MA 02139.

§ Current address: Laboratoire de Biochimie Physique et des Biopolymères, Université Catholique de Louvain, Bâtiment Lavoisier, 1/1B Place L. Pasteur, B-1348 Louvain-la-Neuve, Belgium.

10.1021/bi9827971 CCC: $18.00
Published on Web 05/26/1999

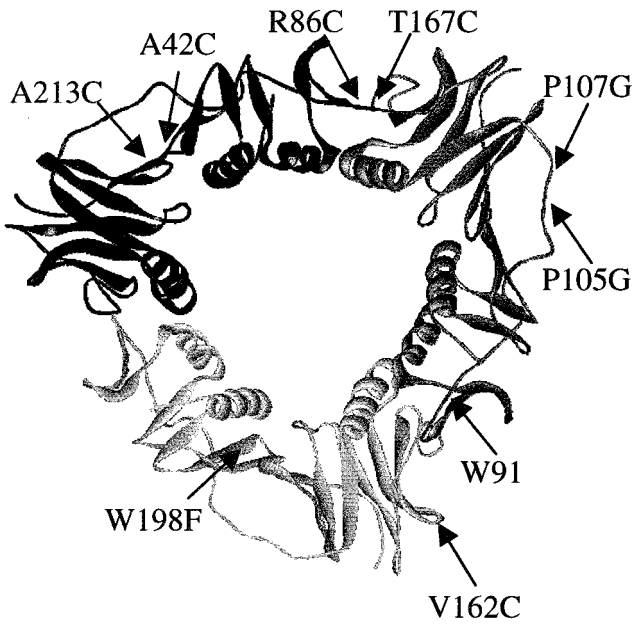

FIGURE 1: X-ray crystal structure of gp45 and locations of mutations used in this study. For clarity, each mutation is only shown once per trimer. The location of W91 is also shown.

shown that (1) multiple conformational changes occur in gp45 during the loading process (*8*−*10*) and (2) subunit exchange associated with transient opening of the gp45 ring is not responsible for its loading onto DNA (requiring another mechanism to be responsible for loading a closed protein circle onto DNA) (*11*). Subunit exchange in gp45 appears instead, however, to be the mechanism for holoenzyme disassembly, but cooperative versus noncooperative models of gp45 assembly from monomers were not decisively distinguished (*11*).

Analytical ultracentrifugation has also been employed to characterize the structure of gp45. The state of oligomerization (trimer) and molecular mass (77 000 Da) were demonstrated by equilibrium measurements, and the trimer was shown to be very asymmetric by velocity sedimentation measurements. Making the assumption that gp45 is a prolate ellipsoid, the axial ratio was calculated to be 6:1 (*12*). The X-ray crystal structure of gp45 confirms the state of oligomerization and molecular mass, but shows that the assumption of a 6:1 prolate ellipsoid is not consistent with the torus that was found (see Figure 1).

In this paper, we have undertaken analytical ultracentrifugation and fluorescence experiments in combination with hydrodynamic modeling to (1) determine the constant for dissociation (K_d) of the gp45 trimer into monomers, (2) ascertain whether the assembly of the trimer from monomers is cooperative or noncooperative, (3) measure the distances across the subunit interfaces of gp45, and (4) probe the solution structure of the trimer. We have constructed mutants of gp45 with changes in a proline-rich loop region (amino acids 100−110) that alter the flexibility of the loop, a possible pivot point for opening the circular gp45 by gp44/62, as well as mutants with intra- and intersubunit disulfide cross-links that alter the solution structure of the gp45 trimer. We have found that the gp45 trimer assembles cooperatively from monomers with motion about the loop region being important for loading gp45 onto DNA. Surprisingly, gp45 apparently exists as an open trimeric complex in solution.

MATERIALS AND METHODS

Materials. Oligonucleotides were synthesized on an Expidite 8909 DNA synthesizer (PerSeptive Biosystems, Framingham, MA) and deprotected according to the protocol provided by the manufacturer. PCR primers were passed through Sephadex G25 before use. DNA substrates were purified on 20% denaturing polyacrylamide gels, extracted from the gel using a crush and soak procedure (*13*), and desalted using a C18 Sep-Pak (Waters, Milford, MA). 3′-Biotin-labeled oligonucleotides were prepared using a BioTEG CPG column obtained from Glen Research (Sterling, VA). CPM[1] was obtained from Molecular Probes (Eugene, OR). Oligonucleotides were 5′-end labeled with [γ-^{32}P]ATP (New England Nuclear, Boston, MA) and T4 polynucleotide kinase (Amersham, Arlington Heights, IL). T4 DNA ligase was obtained from GibcoBRL (Gathersberg, MD). All restriction enzymes were obtained from New England Biolabs (Beverly, MA). All other chemicals were of analytical grade or better.

Cloning and Protein Purification. The following PCR primers were used in the preparation of the gp45 mutants described in the manuscript: (A) 5′-GCG GAA TTC CAT ATG AAA CTG TCT AAA GAT, (B) 5′-GCG GAA TTC GGA TTC CTA TTA AAA ATC GTG GGT, (C) 5′-TCC TAA TAA AGG TAT ACC ATT CCC GGT A, (D) 5′-TAC CGG TGG TAT ACC TTT ATT AGG A, (E) 5′-TCC TAA TAA ACC GAT CGG ATT CCC GGT A, (F) 5′-TAC CGG GAA TCC GAT CGG TTT ATT AGG A, (G) 5′-CCA AAA AAT TGA GCA TGC ATC AGC AAT, (H) ATC ACC AAG ACA CAA AGA GTA TTT AAC ACG, (I) 5′-GCA ATT TAC GAT TTG AAC GGT TTT CTC GG, (J) 5′-GTC AGA AAT ATT GCA TTC CGC ATA AGT, (K) 5′-GAA GGT GAA CAT TGC AAT TAT GTG GTA, (L) 5′-GAG TCA AAG AGT ATT TAC AAC GGG TCA GAG C, and (M) 5′-TTG TTT ACC TTT CGC GAA AAG CAG AAG TTT.

The P105G mutant was constructed by PCR using T4 genomic DNA (Sigma, St. Louis, MO) and Deep Vent$_R$ DNA Polymerase (New England Biolabs). Primers A and D yielded fragment AD, and primers B and C yielded fragment BC. Overlap-extension PCR of fragments AD and BC with primers A and B yielded full-length 45 with the P105G mutation as well as a new *Bst*Z17 I site. The full-length fragment was digested with *Nde*I and *Bam*HI and ligated into pET26b similarly digested with *Nde*I and *Bam*HI to form pET26b-45-P105G. Likewise, the P107G mutant was constructed using primers A and F yielding fragment AF and primers B and E yielding fragment BE. Overlap-extension PCR of fragments AF and BE with primers A and B yielded full-length 45 with the P107G mutation as well as a new *Pvu*I site that was ligated into pET26b as above to form pET26b-45-P107G.

R86C and T167C mutations were independently prepared by overlap extension of fragments AG and BI (R86C with a

[1] Abbreviations: bio, biotin; bp, base pairs; CPM, 7-diethylamino-3-(4′-maleimidylphenyl)-4-methylcoumarin; dNTP, deoxynucleotide triphosphate; DTNB, 5,5′-dithiobis(2-nitrobenzoic acid); DTT, dithiothreitol; EDTA, ethylenediaminetetraacetic acid; FRET, fluorescence-resonance energy transfer; Hepes, 4-(2-hydroxyethyl)-1-piperazineethanesulfonic acid; $S°$, sedimentation coefficient at infinite dilution; $S_{20,w}$, sedimentation coefficient at 20 °C in pure water; $S_{25,b}$, sedimentation coefficient at 25 °C in buffer b; SDS−PAGE, sodium dodecyl sulfate−polyacrylamide gel electrophoresis; Tris, tris(hydroxymethyl)aminomethane; TNB, 5-thio-2-nitrobenzoic acid.

new *Sph*I site) and fragments AH and BI (T167C with an *Ssp*I site removed), followed by ligation into pET26b yielding pET26b-45-R86C and pET26b-45-T167C, respectively. To form the double mutant, pET26b-45-R86C and pET26b-45-T167C were digested with *Bbs*I to form five fragments (3548, 1326, 388, 360, and 339 bp), with the T167C mutation in the 3548 bp fragment and the R86C mutation in the 1326 bp fragment. *Bbs*I cuts outside its nonpalindromic recognition sequence and yields unique four-base overhangs for each of the five fragments, allowing religation to form the parent plasmid without scrambling or inversion. The 3548 bp fragment from pET26b-45-T167C, the 1326 bp fragment from pET26b-45-R86C, and the 388, 360, and 339 bp fragments were mixed and ligated to form pET26b-45-R86C/T167C.

The A42C/A213C double mutant was constructed by the megaprimer method (*14*) using fragments AJ and BK as megaprimers with T4 genomic DNA as the template. This full-length fragment was ligated into pET26b as above to form pET26b-45-A42C/A213C, encoding new *Bsm*I and *Bsr*DI sites along with the A42C and A213C mutations, respectively.

The A42C/V162C/W198F/A213C mutant was constructed stepwise from pET26b-45-A42C/A213C. Fragments AL and BI were made by PCR using pET26b-45-A42C/A213C as a template. Overlap extension of these fragments with primers A and B followed by ligation into pET26b formed pET26b-45-A42C/V162C/A213C that also removed an *Ssp*I site near the V162C mutation. Fragments AM and BI were then made by PCR using pET26b-45-A42C/V162C/A213C as a template. Overlap extension of these fragments with primers A and B followed by ligation into pET26b formed pET26b-45-A42C/V162C/W198F/A213C that contained a new *Nru*I site near the W198F mutation.

The V162C/W198F double mutant was constructed from fragments AM and BI made by PCR using pET26b-45-V162C (*11*) as a template. Overlap extension PCR of these fragments followed by ligation into pET26b formed pET26b-45-V162C/W198F that contained a new *Nru*I site near the W198F mutation.

All of the above mutant plasmids were transformed into the *E. coli* strain DH5α, and colonies screened with the appropriate restriction enzyme(s). All mutations were confirmed by DNA sequencing. Following transformation into the *E. coli* strain BL21 (DE3), gp45 mutants were purified as described below.

Wild-type gp45, gp44/62, and exonuclease-deficient gp43 were purified as previously described (*15*−*17*). Mutant forms of gp45 were expressed from the above-described pET vectors as previously described (*15*). The A42C/V162C/W198F/A213C and V162C/W198F mutants were expressed at 25 °C for 24 h to improve solubility. Protein concentrations were determined by a Bradford protein assay (Bio-Rad, Hercules, CA).

Disulfide Cross-Linking and Fluorescent Labeling of Gp45 Mutants. Disulfide cross-links (intrasubunit and intersubunit) were formed using the following procedure: mutant gp45 was dialyzed versus degassed 20 mM Hepes, pH 7.0, 50 mM NaCl, 1 mM EDTA, and 10% glycerol (storage buffer) and then treated with 1 mM DTNB at 4 °C for 6 h to form the thionitrobenzoate mixed disulfide. This mixture was dialyzed versus storage buffer to remove excess DTNB and the protein then diluted with storage buffer to 2.5 μM or less. DTT was added in aliquots at 25 °C over 1 h, with the final DTT concentration equal to 1.5 equiv/gp45 cysteine. This mixture was allowed to react further at 4 °C for 12 h. The cross-linked protein was then concentrated and stored at −70 °C. During this cross-linking process, some of the protein was found to precipitate (20−50% for the R86C/T167C and A42C/A213C mutants and as much as 90% for the A42C/V162C/W198F/A213C mutant). Dilution of the protein prior to DTT addition helped to prevent but not eliminate precipitation, suggesting that intermolecular cross-linking or aggregation was responsible for precipitation. Only the soluble fraction was used for further analysis. In an attempt to protect the protein, cross-linking was carried inside a glovebag under a blanket of argon using only degassed buffers. Even under these carefully controlled conditions, protein precipitation could not be avoided.

SDS−PAGE analysis demonstrates that about 90% of R86C/T167C was cross-linked to the linear trimer and nearly 100% of A42C/A213C formed intrasubunit cross-links (intrasubunit cross-links run faster than wild-type gp45 on SDS−PAGE). The number of free thiols remaining was verified by titration with DTNB (*18*) and was consistent with the SDS−PAGE result.

To label the A42C/V162C/W198F/A213C mutant with CPM, the protein solution following DTNB/DTT cross-linking and concentration as described above was dialyzed versus storage buffer to remove excess DTT, DTNB, and TNB and diluted with 0.1 vol of DMF. An excess (10 equiv) of CPM was added in aliquots at 25 °C over 2 h and allowed to react further at 25 °C for 4 h. The protein solution was dialyzed versus storage buffer to remove excess CPM and divided into two fractions. One fraction was treated with 20 mM DTT to reduce the intrasubunit disulfide bonds. Both fractions were incubated at 37 °C for 18 h and then stored at −70 °C. The V162C/W198F double mutant was similarly labeled with CPM at 4 °C for 18 h. The protein solution was dialyzed versus storage buffer to remove excess CPM and stored at −70 °C. For both mutants, the amount of labeling was determined by UV-vis spectroscopy using $\epsilon_{384} = 33\,000\ \text{cm}^{-1}\ \text{M}^{-1}$ to quantitate the CPM chromophore. The number of free thiols at each step was verified by DTNB titration (un-cross-linked A42C/V162C/W198F/A213C 7.8, calculated 9.0; cross-linked A42C/V162C/W198F/A213C 2.6, calculated 3.0; cross-linked A42C/V162C/W198F/A213C−CPM 0.1, calculated 0.0; V162C/W198F 3.1, calculated 3.0; V162C/W198F−CPM 0.3, calculated 0.0). Un-cross-linking of A42C/V162C/W198F/A213C−CPM was verified by SDS−PAGE (excess DTT prevented DTNB titration).

ATPase and Strand-Displacement Assays. The coupled spectrophotometric ATPase assay was conducted with a biotinylated forked primer-template (bio34/62/36) as described previously (*5*, *19*). The bio34/62/36 substrate was constructed by annealing 1.0 equiv of the bio62-mer template with 1.0 equiv of the 34-mer primer, purifying on a non-denaturing polyacrylamide gel, and adding 1.1 equiv of the 36-mer fork. To determine the basal rate of ATP hydrolysis, gp45 and gp44/62 (250 nM final each) were added to a cocktail containing 1 mM ATP, 3.3 mM phosphoenolpyruvate, 200 μM NADH, 500 μM streptavidin, and approximately 1 unit each of pyruvate kinase and lactate

dehydrogenase in 20 mM Tris, pH 7.5, 150 mM potassium acetate, and 10 mM magnesium acetate (complex buffer). Bio34/62/36 was added (250 nM final) and the pre-shut-down rate of ATP hydrolysis obtained. Finally, gp43 (250 nM final) was then added and the post-shut-down rate of ATP hydrolysis obtained.

The strand-displacement assay was conducted as previously described (*20*) in a benchtop format. The DNA substrate was constructed by labeling 1.0 equiv of the 34-mer primer on the 5′-end with ^{32}P and annealing to 1.0 equiv of the bio62-mer template and 1.5 equiv of the 36-mer fork. Briefly, 550 nM gp45, 550 nM gp44/62, 500 nM bio34/62/36, 1 μM streptavidin, and 1 mM ATP were incubated in 45 μL of complex buffer for 30 s. A 5 μL aliquot of a mixture of gp43 (100 nM final) and dCTP (10 μM final) was added, and this mixture incubated for an additional 30 s. During this time, 5 μL were removed and quenched into aqueous HCl. A 5 μL aliquot of a mixture of salmon sperm DNA trap (0.75 mg/mL final) and the final three dNTPs (10 μM each final) was then added, and 5 μL aliquots of this final mixture quenched at 10 and 30 s into aqueous HCl. The quenched samples were extracted with phenol:chloroform:isoamyl alcohol (25:24:1) and neutralized with aqueous NaOH. DNA products were separated on a 16% denaturing polyacrylamide sequencing gel and visualized by phosphorimagery. The ratio of strand-displaced full-length DNA products (56−62-mers) to unextended and singly extended DNAs (34−35-mers) was used to calculate the concentration of active holoenzyme present (90 nM theoretical maximum).

Sedimentation Equilibrium Analysis. Sedimentation equilibrium measurements of mutant and wild-type forms of gp45 were performed using a Beckman (Fullerton, CA) XL-I Analytical Ultracentrifuge in absorbance mode. Data were acquired using the supplied XL-I acquisition software. All experiments were performed at 25 °C in 25 mM potassium phosphate, pH 7.4, and 200 mM KCl (ultracentrifugation buffer). Protein samples were dialyzed against ultracentrifugation buffer at 4 °C for at least 12 h immediately before analysis. A six-channel centerpiece allowed simultaneous acquisition of a broad concentration range (from 100 nM to 9.7 μM) while monitoring at wavelengths (220, 230, or 280 nm) appropriate for the protein concentration. Data were obtained at rotor speeds of 14 000, 16 000, and 18 000 rpm. Equilibrium was considered reached when two consecutive sets of data taken 2 h apart were completely superimposable. Following collection of equilibrium data, the rotor speed was increased to 36 000 rpm to deplete the meniscus, allowing experimental determination of the baseline at the meniscus.

Data editing was performed using the software package Microcal Origin (v3.78, Microcal Software, Northampton, MA). Local and global nonlinear least-squares analysis techniques were employed using the program WinNonlin [v1.03 (*21*)] to extract solution molecular weight and self-association constants, which were then transformed into K_d values.

Sedimentation Velocity Analysis. Sedimentation velocity experiments were performed in two-channel centerpieces using the Beckman XL-I Analytical Ultracentrifuge described above. Mutant and wild-type forms of gp45, freshly dialyzed into ultracentrifugation buffer, were analyzed over an extensive concentration range (100 nM to 19 μM) at a rotor speed of 36 000 rpm at 25 °C. To calculate the sedimentation coefficient at each concentration ($S_{25,b}$), the data were analyzed using the transport method (*22*) and the second moment method (*23*) contained in the Microcal Origin software package. Further verification of sedimentation coefficients was accomplished by the van Holde−Weischet method (*24*) in the UltraScan II software package (v3.0). $S^\circ_{20,w}$ was determined by plotting $S_{25,b}$ versus concentration, extrapolating to infinite dilution to determine $S°$, and then correcting these values to 20 °C in pure water by using the following equation (*25*):

$$S^\circ_{20,w} = S^\circ \frac{(1 - \bar{\nu}\rho)_{20,w}(\eta_{T,b})}{(1 - \bar{\nu}\rho)_{T,b}(\eta_{20,w})} \quad (1)$$

where $\bar{\nu}_{25}$ (the partial specific volume of gp45 at T = 25 °C) is 0.7430 mL/g, $\bar{\nu}_{20}$ is 0.7409 mL/g, $\rho_{20,w}$ (the density of pure water at 20 °C) is 0.9982 g/mL, $\rho_{25,b}$ (the density of buffer b at 25 °C) is 1.009 68 g/mL for ultracentrifugation buffer, $\eta_{20,w}$ (the viscosity of pure water at 20 °C) is 0.010 02 poise, and $\eta_{25,b}$ is 0.008 948 9 poise for ultracentrifugation buffer.

Steady-State Fluorescence Spectroscopy. Steady-state fluorescence spectroscopy and steady-state polarization spectroscopy were performed on a SLM-8000C spectrofluorometer (SLM Instruments, Urbana, IL) using an ozone free 450 W xenon arc lamp as the source. All calculations were performed using Microsoft (Redmond, WA) Excel97 and KaleidaGraph 3.0 (Synergy Software, Reading, PA). Fluorescence experiments were carried out using 0.25−2.0 μM gp45 in complex buffer. Protein concentrations of labeled and unlabeled gp45 were determined by a Bradford protein assay immediately before use to ensure accurate analysis as described below. All solutions were equilibrated at 25 °C for 30 min prior to analysis. Fluorescence intensities were determined by integrating the area of the tryptophan emission peak between 300 and 420 nm.

To calculate the distance, R, between the W91 donor and V162C−CPM acceptor, the Förster equation was used (*26*):

$$R = R_0\left(\frac{1 - E}{E}\right)^{1/6} \quad (2)$$

Only two unknown parameters are required: R_0, the Förster distance (where energy transfer is 50% efficient), and E, the transfer efficiency. The quenching of tryptophan fluorescence was first used to determine E (*27*):

$$E = R_0\left(\frac{1}{\nu}\right)\left(1 - \frac{F_{DA}}{F_D}\right) \quad (3)$$

where ν is the fraction of gp45 in trimeric form [calculated from the dissociation constant K_d determined by fluorescence (*11*)], F_{DA} is the fluorescence intensity of acceptor-labeled gp45, and F_D is the fluorescence intensity of unlabeled gp45.

The determination of R_0 is not as straightforward (*25*). Several parameters must be experimentally determined and R_0 then calculated from the following formula:

$$R_o = (0.211\phi_D\kappa^2\eta J)^{1/6} \quad (4)$$

where ϕ_D is the quantum yield of the donor, κ^2 is the orientation factor, η is the refractive index of the medium (assumed to be 1.4), and J is the overlap integral between

the fluorescence spectrum of the donor and the absorption spectrum of the acceptor. The overlap integral, *J*, was calculated from the following formula:

$$J = \int F_n(\lambda) \times \epsilon_A(\lambda) \times \lambda^4 \times \partial\lambda \quad (5)$$

where $F_n(\lambda)$ is the fluorescence intensity of the donor (in the absence of the acceptor) as a fraction of the total integrated intensity, $\epsilon_A(\lambda)$ is the extinction coefficient of the acceptor, and λ is the wavelength of overlap.

The quantum yield of the donor (ϕ_D) was obtained by determining both the absorption and fluorescence emission spectra of a donor-only gp45 sample and of a reference compound (L-tryptophan). The quantum yield was calculated from the following formula (*28*):

$$\phi_D = \phi_T\left(\frac{F_D}{F_R}\right)\left(\frac{A_R}{A_D}\right) \quad (6)$$

where ϕ_r is the quantum yield of the reference compound (*29*), F_D and F_R are the fluorescence emission intensities of the donor and the reference compound, respectively, and A_D and A_R are the absorption intensities of the donor and reference compound, respectively.

One of the most problematic parameters to determine distances from FRET experiments is the orientation parameter, κ^2, which relates the relative orientation of the donor/acceptor pair. This parameter can take any value between 0 and 4 (*30*). For a freely rotating probe, κ^2 is assumed to have a value of 2/3. Steady-state fluorescence polarization spectroscopy, which allows anisotropy to be calculated, can be used to determine the rotational freedom of the probe and, therefore, if the assumption of $\kappa^2 = 2/3$ is valid. Polarization measurements were made with Glan−Thompson calcite prism polarizers. For each probe, four fluorescence intensities, *I*, are necessary: I_{HV}, I_{HH} , I_{VH}, and I_{VV}, where the subscripts indicate the orientation of the polarizer (horizontal or vertical). The first subscript position refers to the excitation polarizer, and the second position refers to the emission polarizer. An average of 10 measurements was used to determine each parameter. Anisotropy, *A*, was calculated from the following formula:

$$A = \left(I_{VV} - \left(\frac{I_{HV}}{I_{HH}}\right)I_{VH}\right) \Big/ \left(I_{VV} + 2\left(\frac{I_{HV}}{I_{HH}}\right)I_{VH}\right) \quad (7)$$

Both the tryptophan and CPM in gp45 have anisotropy values below 0.3, and therefore, the error in the measured distance introduced by assuming $\kappa^2 = 2/3$ is less than 10% (*31*).

To investigate the tryptophan environments in the various mutant forms of gp45, the quenching of tryptophan fluorescence by KI was determined. Protein aliquots (250 nM) were placed in complex buffer, and increasing amounts of KI (0−0.2 M) were added. The intensity of the tryptophan fluorescence was determined for each sample. The data were plotted on a linear Stern−Volmer graph (data not shown) (*32*).

Hydrodynamic Modeling. Molecular modeling was performed using Quanta (v97, Molecular Simulations, San Diego, CA) running on a Silicon Graphics Indigo^2 (Mountain View, CA). The crystal structure of gp45 was modified in the following way to form the in-plane and out-of-plane models: the dihedral angles C104−Cα104−N104−C103 (rotated from −125° to −153°) on subunit 3 and N107−Cα107−C107−N108 (rotated from 103 to 74°) on subunit 2, respectively, were rotated to cause the V162/W91 distance at the opposite (180° away) interface to open from 14 to 38 Å to match the fluorescence result. The adjacent subunit interfaces were held fixed during these transformations. The puckered model required changes in three dihedral angles: (1) C103−Cα103−N104−C103 on subunit 1 was rotated from −81 to −41°, (2) N107−Cα107−C107−N108 on subunit 2 was rotated from 103 to 63°, and (3) Cα107−N107−C106−Cα106 on subunit 3 was rotated from 180 to −120°, in all cases holding the interfaces between subunits 1 and 3 and between subunits 2 and 3 fixed. Structures were not energy minimized following these transformations, and PDB files without hydrogen atoms were then made from these structures.

The program AtoB (*33*) was then used to make assemblies of spherical beads from the PDB files, with the input resolution at 5 Å and assuming no hydration. Because of the input limits of AtoB, each subunit was independently transformed into beads, and the three resulting files combined into an assembly of about 560 beads. This assembly of beads was then used as input for the program HYDRO (*34*), modified to allow this number of beads, to predict sedimentation coefficients. These sedimentation coefficients were corrected for hydration [predicted from the amino acid content (*35*)] according to the following relationship (*36*):

$$S_C = S_H\left[\left(\frac{d}{\bar{\nu}\rho}\right) + 1\right]^{-1/3} \quad (8)$$

where S_C is the corrected sedimentation coefficient, S_H is the sedimentation coefficient predicted by HYDRO, and *d* is the protein hydration.

RESULTS

Construction of Gp45 Mutants. Upon inspection of the gp45 X-ray crystal structure (Figure 1), each monomer appears to have two domains connected via a proline-rich loop (amino acids 100−110). This loop provides a potential pivot point for opening the closed structure and allowing the DNA access to the interior of the ring. To probe the importance of the proline-rich loop region of gp45 for loading onto DNA and how it influences the solution structure, several mutants of gp45 were constructed (see Figure 1 for spatial locations). The importance of the central two prolines in the loop was addressed by individually mutating them to glycine (P105G and P107G).

To investigate changes in the solution conformation of gp45 caused by introducing disulfide cross-links to constrain the structure, two double mutants were constructed. A covalently linked trimer was formed by introducing two cysteines (R86C/T167C) at positions that reside across the subunit interface from one another, followed by disulfide bond formation using sequential treatment with excess DTNB and 1.5 equiv of DTT/thiol. Only two of the possible three disulfides were formed per trimer as evidenced by titration of free thiols with DTNB (data not shown). The inability to form the final disulfide suggests that these two thiols are either in the wrong conformation for disulfide formation or the distance between them is greater than the distance between the two pairs of thiols that can be cross-linked. An

Table 1: Activities of Wild-Type and Mutant Forms of Gp45

gp45 species	ATPase (nM s^{-1})[a] gp45 and gp44/62[b]	gp45, gp44/62, and DNA[c]	gp45, gp44/62, DNA, and gp43[d]	strand displacement (nM)[e]
wild-type	23	227	17	86
P105G	72	245	90	81
P107G	284	807	351	75
U−R86C/T167C[f]	62	321	72	80
X−R86C/T167C	14	128	24	50
U−A42C/A213C	58	244	38	94
X−A42C/A213C	13	196	14	46
U−A42C/V162C/W198F/A213C	29	260	31	78
U−A42C/V162C/W198F/A213C−CPM	15	238	22	84
X−A42C/V162C/W198F/A213C	12	284	34	47
X−A42C/V162C/W198F/A213C−CPM	10	196	9.9	47
V162C/W198F	24	322	24	67
V162C/W198F−CPM	8.6	117	5.6	76
none	N/A	N/A	N/A	0.5

[a] ATPase assays contained 250 nM each of gp45, gp44/62, DNA, and gp43. Assays were performed by incubating the ATPase cocktail (see Materials and Methods) with gp45 and gp44/62, then adding DNA after 2 min, then adding gp43 after an additional 2−5 min and rates calculated for each step. Experimental reproducibility is typically ±10%. [b] Called the basal rate of ATP hydrolysis in the text. [c] Called the pre shut-down rate of ATP hydrolysis in the text. [d] Called the post shut-down rate of ATP hydrolysis in the text. [e] Strand displacement assays contained 100 nM gp43, 500 nM radiolabeled DNA, 550 nM gp45, 550 nM gp44/62, and 10 μM dCTP in a volume of 50 μL. Before addition of the remaining dNTPs and salmon sperm DNA trap, 5 μL was withdrawn for a zero point. The theoretical maximum amount of strand displacement is therefore 90 nM. Experimental reproducibility is typically ±10%. [f] U, un-cross-linked. X, cross-linked. N/A, not applicable; only the strand displacement assay was performed without gp45.

intrasubunit disulfide was formed between the two domains of each gp45 monomer by introducing two cysteines (A42C/A213C) that reside across from one another below the loop region, followed by oxidation as above. In this case, all three possible disulfides per trimer were formed as evidenced by observing quantitative conversion to the intrasubunit cross-linked species by SDS−PAGE analysis (the intrasubunit disulfide runs faster than wild-type gp45 on SDS−PAGE) and no further reaction with DTNB (data not shown).

To measure the distance across the subunit interface using fluorescence-resonance energy transfer (FRET), a tetramutant (A42C/V162C/W198F/A213C) was constructed that could form the intrasubunit disulfide cross-link as above and allowed a fluorescent label to be placed at V162C. A FRET signal was previously seen across the subunit interface between the donor W91 and the acceptor V162C labeled with a fluorophore (*11*). To facilitate analysis, the second tryptophan in each gp45 monomer (W198) was mutated to a nonfluorescent phenylalanine. As above, the tetramutant was cross-linked by sequential treatment with DTNB and DTT and labeled with CPM, and in some cases, cross-links were reduced with additional DTT. SDS−PAGE, DTNB titration, and UV-vis spectroscopy confirmed cross-linking, the correct number of free thiols at each step, and the presence of 3 fluorescent labels/trimer, respectively (data not shown). Additionally, the double mutant V162C/W198F was constructed to provide confirmation on the W91 to V162C−CPM distance as measured by FRET. This mutant lacks the intrasubunit disulfide cross-link found in the tetramutant.

ATPase and Strand Displacement Assays. The activities of wild-type gp45 and the above-described mutants were checked by determining their ability to stimulate ATP hydrolysis by gp44/62 using a coupled spectrophotometric assay (*19*) and to promote DNA strand displacement synthesis by gp43 using a radiolabeled primer in a forked primer/template DNA substrate (*20*). As shown in Table 1, wild-type gp45 alone weakly stimulated ATP hydrolysis by gp44/62 (a basal rate of 23 nM s^{-1}), but upon addition of DNA, ATP hydrolysis was strongly stimulated (a pre-shut-down rate of 227 nM s^{-1}). Addition of gp43 decreased the rate of ATP hydrolysis (a post-shut-down rate of 17 nM s^{-1}), presumably by sequestering gp45 into the holoenzyme complex bound to DNA. In all cases, the basal rate was very close to the post-shut-down rate, as would be expected for quantitative formation of a holoenzyme complex. Further addition of gp43 beyond 1 equiv as expected did not decrease the observed rate of ATP hydrolysis for wild-type gp45 or two mutants (cross-linked A42C/A213C and P107G; data not shown), consistent with a 1:1 gp45:gp43 holoenzyme complex.

CPM-labeled and unlabeled forms of the un-cross-linked tetramutant (A42C/V162C/W198F/A213C) had pre-shut-down rates (238 and 260 nM s^{-1}, respectively) similar to wild-type gp45 (227 nM s^{-1}). Two of the double mutants (R86C/T167C and A42C/A213C) when un-cross-linked had basal (62 and 58 nM s^{-1}, respectively) and pre-shut-down rates (321 and 244 nM s^{-1}, respectively) somewhat higher than wild-type gp45. Cross-linking these mutants generally caused a decrease in all three of the measured ATP hydrolysis rates. This behavior was not observed for the tetramutant, but there generally was a moderate decrease in activity upon labeling with CPM in both cross-linked and un-cross-linked forms. Labeling of V162C/W198F with CPM caused a decrease in the pre-shut-down rate, from 322 to 117 nM s^{-1}.

The loop mutant P105G had a pre shut-down rate close to wild-type gp45, while the basal and shut-down rates were found to be slightly higher than wild-type gp45. However, P107G was very different from wild-type gp45. The basal and pre-shut-down rates were significantly higher (284 and 807 nM s^{-1}, respectively), and upon addition of gp43, the post-shut-down rate only dropped to 351 nM s^{-1}.

The strand displacement assay used a forked primer-template DNA substrate to monitor processive DNA synthesis. Any polymerase that releases from the DNA substrate,

Table 2: Molecular Masses and K_d Values Determined by Equilibrium Ultracentrifugation and $S^\circ_{20,w}$ Values Determined by Velocity Sedimentation

gp45 species	molecular masses (Da)[a]	RMS deviation[b]	K_d (μM^2)[c]	RMS deviation[d]	$S^\circ_{20,w}$ ($s \times 10^{-13}$)[e]
wild-type	69 000 ± 8000	4.8×10^{-4}	0.21 (0.60−0.077)	4.4×10^{-4}	4.0 ± 0.1
P105G	69 000 ± 2000	3.4×10^{-5}	0.12 (0.21−0.071)	5.6×10^{-5}	4.4 ± 0.1
P107G	71 000 ± 9000	5.3×10^{-4}	0.16 (0.26−0.090)	5.0×10^{-5}	4.6 ± 0.1
X−R86C/T167C[f]	74 000 ± 2000	4.1×10^{-5}	N/A	N/A	4.5 ± 0.1
X−A42C/A213C	74 000 ± 6000	1.7×10^{-4}	0.088 (0.17−0.042)	7.3×10^{-5}	4.8 ± 0.2
X−A42C/V162C/W198F/A213C	70 000 ± 6000	2.3×10^{-4}	0.26 (0.69−0.092)	3.5×10^{-4}	ND
X−A42C/V162C/W198F/A213C−CPM	69 000 ± 5000	2.3×10^{-4}	0.32 (0.82−0.12)	4.0×10^{-4}	ND

[a] Molecular weight errors are confidence intervals approximately equal to 1 standard deviation as determined by WinNonlin (*21*). [b] Root-mean-square deviation of the data from the molecular weight determination. No systematic variations were observed in the residuals. [c] K_d errors are confidence intervals approximately equal to 1 standard deviation as determined by WinNonlin (*21*). [d] Root-mean-square deviation of the data from the K_d determination. No systematic variations were observed in the residuals. [e] Intercept of $S_{20,w}$ versus concentration plot (see Figure 4). [f] X, cross-linked. ND, not determined. N/A, nonapplicable; cross-linked R86C/T167C is a covalently linked trimer.

either upon reaching the end of the substrate following completion of polymerization or though dissociation, is trapped with salmon sperm DNA and cannot participate further in DNA synthesis so that the maximum theoretical amount of full-length DNA products is 90 nM. The polymerase alone was not able to displace the forked strand and synthesize full-length DNA products (0.5 nM). Addition of gp45 and gp44/62 resulted in the formation of a complex that was able to displace nearly quantitatively the forked strand and synthesize full-length DNA products (86 nM). Un-cross-linked mutants of gp45 with and without fluorescent labels likewise yielded 78−94 nM full-length DNA products. Cross-linking these mutants resulted in a decrease in the yield of full-length DNA products (46−50 nM). Labeled and unlabeled V162C/W198F and the loop mutants P105G and P107G displayed near wild-type activity, with 67−81 nM full-length DNA products synthesized.

Equilibrium Ultracentrifugation. For wild-type gp45 and most of the mutants, the molecular weight as well as the dissociation constant of the trimer were determined by equilibrium ultracentrifugation experiments. Figure 2 shows a representative plot of a wild-type gp45 (9.7 μM loading concentration) equilibrium experiment. Table 2 shows that our results are in agreement with the earlier ultracentrifugation work where an average molecular mass of 77 000 Da was found (*12*) (74 496 Da calculated from the sequence). For wild-type gp45, a molecular mass of 69 000 Da was found, fully consistent with a trimeric species. Cross-linked R86C/T167C and cross-linked A42C/A213C were very close to the molecular mass calculated from the sequence, both 74 000 Da. The molecular masses of labeled and unlabeled cross-linked mutant A42C/V162C/W198F/A213C and the loop mutants P105G and P107G were likewise fully consistent with trimeric species (69000−71000 Da).

To determine the dissociation constant of the trimer, WinNonlin was used for global fitting of the low concentration data (lower than 1 μM) to both cooperative (monomer ↔ trimer) and noncooperative (monomer ↔ dimer ↔ trimer) models. The noncooperative model failed to converge upon a solution, whereas the cooperative model converged on a solution with low fitting errors. The cooperative dissociation constant for wild-type gp45 was found to be 0.21 μM^2 (confidence interval of 0.60−0.077 μM^2), in good agreement with an earlier fluorescence study that was unable to distinguish cooperative from noncooperative models (*11*). The error limits are confidence intervals determined by

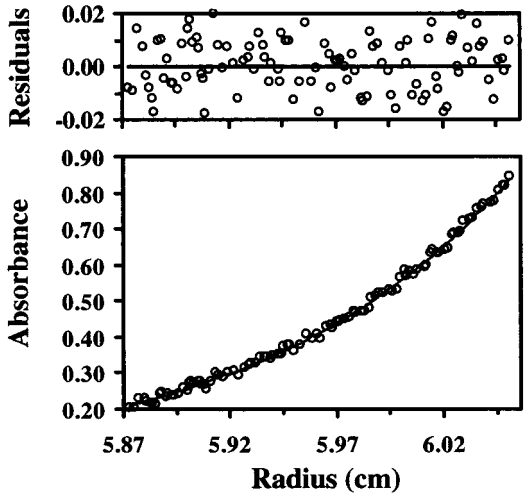

FIGURE 2: Representative equilibrium sedimentation data for molecular weight determination (9.7 μM loading concentration of wild-type gp45 shown as open circles). A global fit to nine data sets (eight data sets not shown) from three protein loading concentrations at three rotor speeds is shown as a solid line, with the residuals due to deviation of the data from this line shown above in the inset.

WinNonlin. They are approximately equal to 1 standard deviation and are nonsymmetric because of the nonlinear algorithm (*21*). For all other mutants, the dissociation constants were found to be nearly indistinguishable (from 0.088 to 0.32 μM^2) from wild-type.

Velocity Ultracentrifugation. The sedimentation coefficients of wild-type gp45 and several mutants were determined over a wide concentration range (0.1−19 μM). Figure 3 shows a representative plot of a wild-type gp45 (19 μM) velocity experiment (part A) as well as analysis of the data using the van Holde−Weischet method (*24*) with the program Ultrascan II (part B). The lines do not converge on the *y*-axis as is observed for symmetric or spherical molecules, but converge to the right of the *y*-axis as is observed for asymmetric or elongated molecules (*37*). A replot of the *y*-intercepts (part C) displays a curved pattern also typical of asymmetric or elongated molecules (*37*). As would be expected (*37*), van Holde−Weischet plots of velocity sedimentation data converge on the *y*-axis for lower protein concentrations [including that used previously (*12*); data not shown].

Figure 4 shows the sedimentation coefficients, corrected to 20 °C in water ($S_{20,w}$) (*25*), as a function of concentration

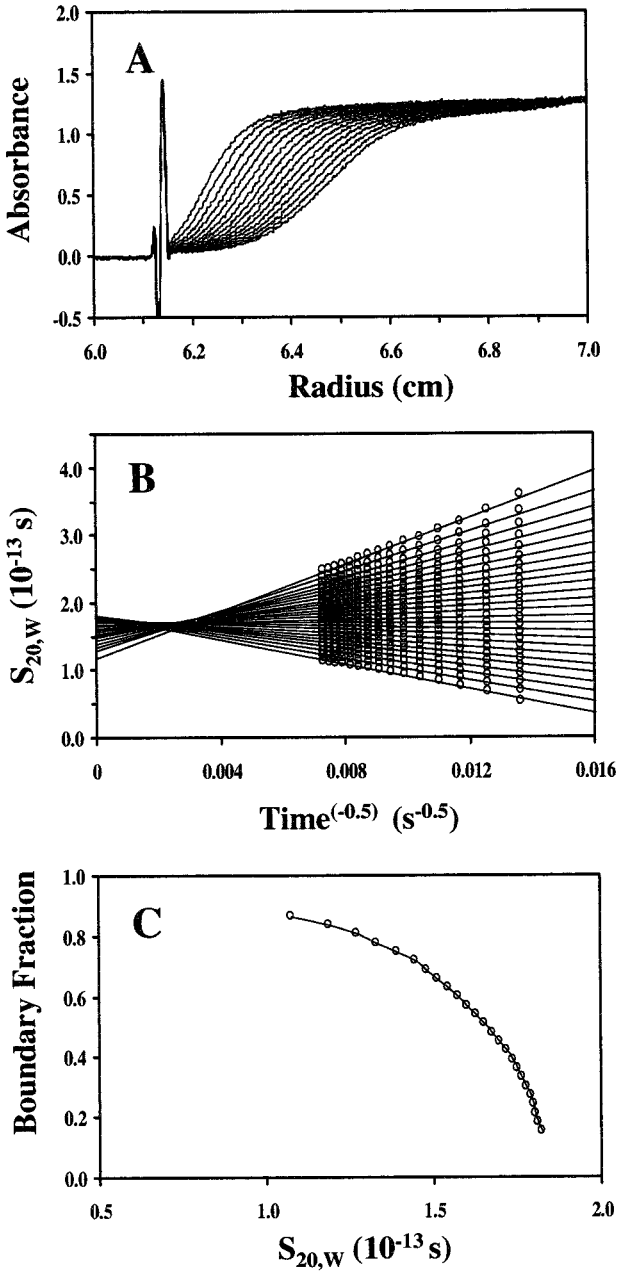

FIGURE 3: Representative velocity sedimentation data (19 μM wild-type gp45). (A) absorbance versus radius for 16 time points between 90 and 328 min; (B) $S_{20,w}$ versus (time)$^{-0.5}$ for 25 boundary fractions using the van Holde−Weischet method of analysis; and (C) boundary fraction versus $S_{20,w}$ using the van Holde−Weischet method of analysis.

for wild-type gp45 and two mutants. The strong concentration dependence of $S_{20,w}$ for wild-type gp45 is again consistent with asymmetric or elongated molecules (*25*). The *y*-intercept of the $S_{20,w}$ versus concentration plot, $S^{\circ}_{20,w}$, for wild-type gp45 is 4.0 ± 0.1 S (see Table 2). Our results are again in complete agreement with the earlier ultracentrifugation study (*12*), where $S_{20,w}$ was found to be 3.9 S when measured at one concentration (0.38 mg/mL or 5.1 μM). At this concentration we find $S_{20,w}$ to be 3.3 S.

However, the $S_{20,w}$ values of cross-linked R86C/T167C and A42C/A213C do not have an appreciable concentration dependence, consistent with symmetric or spherical molecules. $S^{\circ}_{20,w}$ values for cross-linked R86C/T167C and A42C/A213C were found to be 4.5 ± 0.1 and 4.8 ± 0.2 S,

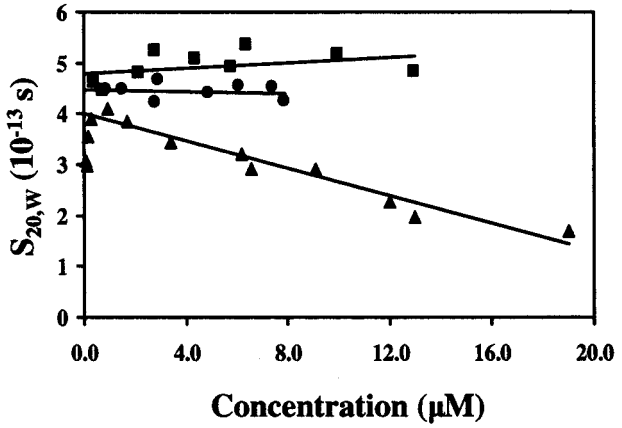

FIGURE 4: $S_{20,w}$ versus concentration for wild-type gp45 (▲), cross-linked R86C/T167C (●), and cross-linked A42C/A213C (■).

respectively. The higher values of $S^{\circ}_{20,w}$ are also consistent with symmetric or spherical molecules (*25*). We investigated whether disulfide formation acts as a conformational switch by reducing cross-linked R86C/T167C and A42C/A213C. Treatment of R86C/T167C and A42C/A213C with 20 mM DTT for 24 h at 25 °C yielded complete reduction of the cross-links as evidenced by SDS−PAGE (data not shown). Unfortunately, this high DTT concentration optically interfered with analysis by ultracentrifugation, so the proteins were subsequently dialyzed into 200 mM KCl, 25 mM potassium phosphate, pH 7.4, and 5 mM DTT, where about 20% of both mutants re-cross-linked as evidenced by SDS−PAGE (data not shown). These mixtures were found to have $S_{20,w}$ values of 3.7 and 4.3 S for 7.4 μM R86C/T167C and 4.1 μM A42C/A213C, respectively, values intermediate between their cross-linked forms and wild-type gp45.

The loop mutants P105G and P107G also show only a weak concentration dependence of $S_{20,w}$, with $S^{\circ}_{20,w}$ (4.4 ± 0.1 and 4.6 ± 0.1 S, respectively) closest to cross-linked R86C/T167C. The increased flexibility of glycine over proline apparently allows the protein to become more symmetric or spherical than wild-type gp45.

Fluorescence. FRET experiments allow fluorescence intensity of a donor−acceptor pair to be related to the distance between them (*38*). The tetramutant A42C/V162C/W198F/A213C was constructed to measure the distance across the subunit interface between the donor W91 and acceptor V162C−CPM. The W198F mutation ensured that there would be only one tryptophan per gp45 monomer. Following the DTNB/DTT procedure (see Materials and Methods), an A42C/A213C disulfide bond was formed, and the V162C position was then labeled with CPM. Half of the cross-linked and labeled protein was subsequently subjected to 20 mM DTT for 16 h to reduce the disulfide bond.

Steady-state fluorescence spectroscopy (Figure 5A) showed that attachment of CPM to the V162C position had a quenching effect on the tryptophan fluorescence of A42C/V162C/W198F/A213C. Concomitantly, a new fluorescence band was observed at 470 nm upon excitation at 280 nm (data not shown). This new band was attributed to energy transfer from tryptophan to CPM. Similar tryptophan quenching (Figure 5B) and CPM sensitization were observed with V162C/W198F−CPM. Tryptophan fluorescence quenching and CPM fluorescence sensitization were more prominent for cross-linked A42C/V162C/W198F/A213C−CPM than

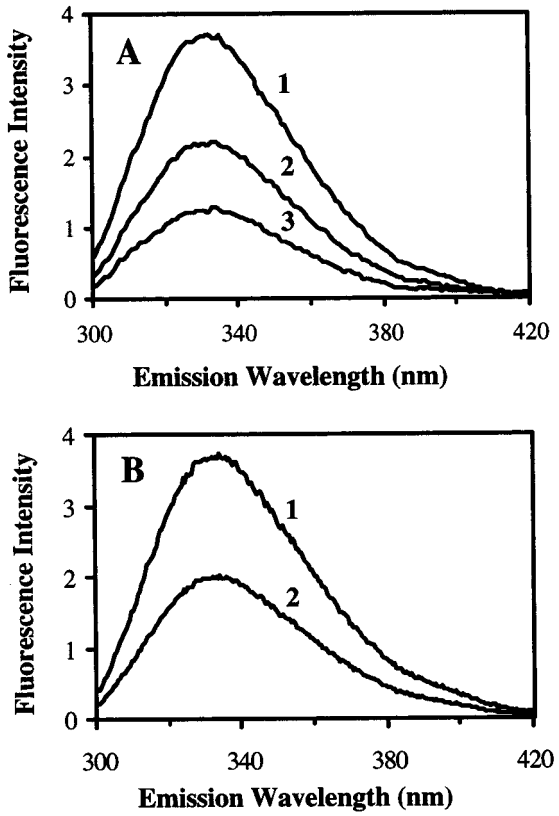

FIGURE 5: (A) Fluorescence spectrum of tryptophan for (1) un-cross-linked, unlabeled A42C/V162C/W198F/A213C; (2) un-cross-linked, CPM-labeled A42C/V162C/W198F/A213C; (3) cross-linked, CPM-labeled A42C/V162C/W198F/A213C and (B) fluorescence spectrum of tryptophan for (1) unlabeled V162C/W198F and (2) CPM-labeled V162C/W198F.

for un-cross-linked A42C/V162C/W198F/A213C−CPM. As a control, 20 mM DTT was shown not to quench or sensitize any fluorescence signals. Additionally, un-cross-linked A42C/V162C/W198F/A213C−CPM was dialyzed versus storage buffer containing 20 mM DTT. Fluorescence spectra before and after dialysis were superimposable, showing that DTT treatment did not release CPM from gp45. The differences in tryptophan quenching, therefore, suggested that W91 and V162C−CPM are closer in space in cross-linked A42C/V162C/W198F/A213C−CPM than in un-cross-linked A42C/V162C/W198F/A213C−CPM.

To calculate the exact distance between W91 and V162C−CPM, the Förster distance, the distance at which half of the donor fluorescence has been transferred to the acceptor (*39*), was determined for this pair. Using the experimental parameters obtained from steady-state measurements [ϕ_D, κ^2, η, J, $F_n(\lambda)$, $\epsilon_A(\lambda)$, λ^4] (*40*), R_0 was determined to be 31 Å for the tryptophan−coumarin pair in A42C/V162C/W198F/A213C. A similar result was obtained from the tryptophan−coumarin pair in V162C/W198F. Our calculation of R_0 for tryptophan and CPM is fully consistent with a previous study that also found a value of 31 Å (*41*).

DISCUSSION

We have cloned and purified several mutants of gp45 to test the importance of the proline-rich loop region that links the two domains of each monomer of gp45. The P105G and P107G mutants allow greater flexibility in the loop region, while R86C/T167C and A42C/A213C allow the introduction of intersubunit and intrasubunit disulfide cross-links, respectively. The cross-link formed in A42C/A213C was intended to inhibit motion between the two domains found within the gp45 monomers. The tetramutant A42C/V162C/W198F/A213C can form this intrasubunit disulfide and can be labeled at V162C with a fluorescent label such that the FRET signal from W91 can be measured across the subunit interface. The double mutant V162C/W198F also allows the W91 to V162C distance to be measured.

The majority of the mutations do not affect the ability of gp45 to stimulate the ATPase activity of gp44/62, the loop mutants P105G and P107G being the notable exceptions. P105G slightly increases the basal and post-shut-down ATPase rates, while P107G dramatically increases all three ATPase rates. The increased flexibility of the loop may be increasing the off rate of gp45 from DNA, requiring gp44/62 to hydrolyze more ATP to maintain gp45 on DNA. The off rate of gp45 from DNA was found to be the slowest step in the overall kinetic mechanism of holoenzyme assembly and disassembly (*42*); increasing this off rate would cause an increase in steady-state ATP hydrolysis by gp44/62 due to an increase in gp45 recycling. The increase in the basal ATP hydrolysis rate of gp44/62 with P107G but without DNA also suggests increased flexibility of the loop and structural changes centered on the loop: gp44/62 has been shown to interact with gp45 in the absence of DNA and cause a conformational change concomitant with ATP hydrolysis (*8*−*10*). If the structural perturbations in the P107G mutant cause more rapid relaxation from the activated conformational state achieved by interaction with the clamp loader, then increased ATP hydrolysis is required to maintain the P107G mutant in the active conformation.

As shown above, the amount of full-length DNA products synthesized by gp43 using P105G and P107G as clamp proteins is nearly identical to wild-type gp45, while the sedimentation velocity experiments suggest that P105G and P107G are more spherical than wild-type gp45. The mechanism of ATPase stimulation by these mutants probably is due to a change in solution conformation and increased loop flexibility, but the change in the holoenzyme off rate is not significant enough to alter the extent of strand displacement from this relatively short stretch of DNA and affect the observed quantities of full-length DNA products. Since this assay was conducted in the presence of excess gp45, it may not be sensitive to subtle changes in the mechanism of the clamp loading process.

The strand displacement assays demonstrate that the various mutant proteins (un-cross-linked, cross-linked, and fluorescently labeled) do not significantly affect the ability to promote strand-displacement DNA synthesis by gp43. All of the cross-linked mutants show slightly decreased amounts of full-length DNA products relative to wild-type gp45, while un-cross-linked mutants as well as the loop mutants show amounts comparable to wild-type gp45 (see Table 1). The near wild-type ATPase and strand-displacement activities of the gp45 mutants suggest that cross-linking and labeling do not significantly alter the conformation or folding of the gp45 trimer since functional interactions with gp44/62, gp43, and DNA can be achieved. Cross-linking of the R86C/T167C mutant does cause the ATPase rate of gp44/62 in the presence of DNA to drop from 321 nM s^{-1} to about one-third the level of the un-cross-linked mutant (128 nM s^{-1}). Since only

one of three subunit interfaces is available for clamp opening and closing, we speculate that the off rate from DNA [shown above to be the slowest step in holoenzyme assembly and disassembly (*42*)] and, therefore, ATP hydrolysis by gp44/62 due to slower gp45 recycling, has dropped to one-third upon cross-linking. We originally envisioned that the intrasubunit cross-link between the two domains of each monomer in the A42C/A213C mutant would restrict the motion between the two domains and inhibit its ability to form a functional holoenzyme. As the ATPase and strand-displacement assays suggest, gp44/62 can overcome this constraint and load cross-linked A42C/A213C onto DNA. As shown below, however, the shape of the trimer formed by cross-linked A42C/A213C is more symmetric or spherical than that of the wild-type trimer.

The molecular mass data obtained in this study is indicative of a trimer for wild-type gp45 as well as all mutants. Our value for wild-type gp45 (69 000 Da) is consistent with the earlier study (77 000 Da) (*12*) as well as the value predicted from the sequence (74 496 Da). We have also determined the K_d of the trimer to be 0.21 μM^2, with all the mutants falling in the range 0.088−0.32 μM^2. The value for wild-type gp45 agrees closely with earlier studies that estimated the K_d using fluorescence (*11*) or gel filtration (*43*), but additionally, we have shown this disassociation to be cooperative. The noncooperative model was eliminated by virtue of the fitting program WinNonlin failing to converge on a solution for this model, as well as the results obtained by velocity sedimentation. Figure 4 shows that $S_{20,w}$ does not begin to decrease due to dissociation until 170 nM trimer. A K_d of 0.21 μM^2 requires that 50% or more of the total protein be trimeric until about 200 nM. At this level, the amount of monomer present should begin to dominate the observed sedimentation coefficient, resulting in a decrease in $S_{20,w}$. Had the noncooperative model been true with the product of the dissociation constants equal to 0.21 μM^2, even at 10 μM only 70% of the protein would be trimeric, with a decrease in $S_{20,w}$ probably observable by 5 μM.

The strong concentration dependence of $S_{20,w}$ and the low $S^\circ_{20,w}$ value (Figure 4) for wild-type gp45 are consistent with the formation of an open complex. Asymmetric or elongated molecules such as DNA (*44*) possess concentration-dependent values of $S_{20,w}$. Unfortunately, the slope of the $S_{20,w}$ versus concentration plot cannot be quantitatively related to the shape of the molecule (*25*). $S^\circ_{20,w}$ values ($S_{20,w}$ corrected to infinite dilution by extrapolation of the $S_{20,w}$ versus concentration plot to zero concentration) that significantly deviate from the maximum value possible for a spherical particle of the same molecular mass also suggests an asymmetric or elongated complex for wild-type gp45. Wild-type gp45 was found to have an $S^\circ_{20,w}$ value of 4.0 S, while the maximum value for a spherical molecule of this molecular mass is 5.3 S (*25*). $S^\circ_{20,w}$ values can be quantitatively related to the shape of the molecule (see below). The formation of a wild-type gp45 open complex, where one subunit interface has come apart, is consistent with the demonstration of an asymmetric or elongated complex, and has been confirmed by FRET experiments (see below).

The concentration independence of $S_{20,w}$ and the higher $S^\circ_{20,w}$ values (Figure 4) for the intrasubunit (A42C/A213C) disulfide cross-linked mutant are more in accord with a closed complex, while the intersubunit (R86C/T167C) disulfide cross-linked mutant may form an intermediate complex between the open (wild-type gp45) and closed (A42C/A213C) complexes. The loop mutants P105G and P107G also appear to fall in this intermediate range. These prolines may be acting as architectural features keeping the wild-type protein in an open complex. The more flexible glycines may allow the complex to become more closed relative to wild-type gp45.

As shown in Figure 5A, cross-linked and un-cross-linked A42C/V162C/W198F/A213C−CPM have tryptophan fluorescence intensities different from each other as well as different from unlabeled A42C/V162C/W198F/A213C. To measure the distance between W91 and V162C−CPM, all changes in fluorescence intensity must be ascribed to changes in energy transfer, rather than changes in tryptophan or CPM environment. To eliminate the possibility that changes in fluorescence intensity were due to changes in the environment surrounding the tryptophan or CPM, unlabeled and CPM-labeled forms of gp45 were analyzed by several methods. First, fluorescence quenching by KI was found to be indistinguishable for the various forms of gp45. All Stern−Volmer graphs were linear from 0 to 200 mM KI (data not shown). The graphs were almost identical and could be fitted to the same linear equation, suggesting that the environment of the tryptophan is identical in all forms of gp45. The linearity of these graphs also reflects the fact that tryptophan environments are indistinguishable (*45*) in the different protein conformations as well as protein oligomeric forms, since gp45 monomers and trimers are present at the protein concentration used in this assay. Second, the tryptophan Stokes shift was identical in all forms of gp45 tested, indicating again that the tryptophan environment is identical in all forms of gp45. Third, the tryptophan fluorescence intensities of cross-linked and un-cross-linked A42C/V162C/W198F/A213C−CPM were nearly identical (1.04:1.00) and the CPM fluorescence intensities (excited at 390 nm) of cross-linked and un-cross-linked A42C/V162C/W198F/A213C−CPM were identical (1.0:1.0). All of these fluorescence data as well as the ATPase and strand-displacement data shown in Table 1 demonstrate that the environments of the tryptophan and CPM are not affected by the labeling of position V162C or by the presence or absence of an intramolecular disulfide bond, and therefore any changes in fluorescence intensity observed in the labeled proteins are due solely to energy transfer.

Table 3 lists the transfer efficiencies for unlabeled and CPM-labeled forms of gp45 and calculated distances between W91 and V162C−CPM for two models: one in which the distance between each of the three subunit interfaces is equivalent and a second in which one interface is open and two are closed (where the distance between the donor and acceptor pair for the closed subunit interfaces is 19 Å, as shown below). Assuming that all three subunit interfaces are equivalently separated, the W91 to V162C−CPM distance was calculated to be 19 Å [plus or minus less than 10% error due to the assumption of $\kappa^2 = 2/3$ (*31*)] for cross-linked A42C/V162C/W198F/A213C−CPM. The X-ray crystal structure of gp45 shows that the distance between donor and acceptor is 14 Å. It appears that the solution structure of cross-linked A42C/V162C/W198F/A213C closely resembles the toroid structure observed in the crystal structure of gp45. On the other hand, assuming that the distance across each

Table 3: Energy-Transfer Efficiencies of CPM-Labeled Gp45 Mutants and Measured Distances between W91 and V162C for Two Structural Models

gp45 species	method	transfer efficiency (E)	distance between W91 and V162C	
			three equivalent interfaces (Å)	open interface[a] (Å)
wild-type	X-ray	N/A	14	N/A
X−A42C/V162C/W198F/A213C−CPM[b]	FRET	0.95	19	N/A
U−A42C/V162C/W198F/A213C−CPM	FRET	0.70	27	38
V162C/W198F−CPM	FRET	0.75	26	35

[a] Assumes two closed interfaces of 19 Å. [b] X, cross-linked. U, un-cross-linked. N/A, not applicable.

of the three subunit interfaces is identical, the W91 to V162C−CPM distance was calculated to be 27 Å for un-cross-linked A42C/V162C/W198F/A213C−CPM. This distance cannot be reconciled with the X-ray crystal structure of gp45: for V162C−CPM to move 27 Å away from W91 without opening the subunit interface, the loop containing V162C must be moved such that contacts with two β sheets and one α helix within its subunit as well as contacts across the subunit interface would be lost. Such unfolding would almost certainly impair the function of gp45, but this is not observed in the activity assays described in Table 1.

Alternatively, one of the subunit interfaces of gp45 may be open and the other two closed. The energy-transfer efficiency of cross-linked A42C/V162C/W198F/A213C−CPM, E_x, is equal to the average transfer efficiency of each closed interface, E_c:

$$E_x = \frac{3E_c}{3} \tag{9}$$

and the energy-transfer efficiency of un-cross-linked A42C/V162C/W198F/A213C−CPM, E_u, is equal to the average energy-transfer efficiency of two closed interfaces ($2E_c$) and one open interface (E_o):

$$E_u = \frac{(2E_c + E_o)}{3} \tag{10}$$

Combining both equations and expressing them as a function of E_o, we obtain

$$E_o = 3E_u - 2E_x \tag{11}$$

To calculate E_o, we assume that the energy-transfer efficiencies (and therefore the W91 to V162C−CPM distances) of the closed interfaces (E_c) in cross-linked and un-cross-linked A42C/V162C/W198F/A213C are identical, yielding an E_o value of 0.20. The W91 to V162C−CPM distance of the open subunit interface is therefore 38 Å, with the two closed subunit interfaces having their W91 to V162C−CPM distances set at 19 Å.

Confirmation of this distance was demonstrated by using the V162C/W198F mutant labeled with CPM (see Figure 5B). This mutant protein is analogous to the un-cross-linked form of the tetramutant. Assuming three equivalent subunit interfaces, FRET experiments yielded a W91 to V162C−CPM distance of 26 Å. As with A42C/V162C/W198F/A213C, this model does not yield a distance that can be reconciled with the X-ray crystal structure of gp45. Using the second model (one open and two closed subunit interfaces), E_o was calculated to be 0.35. The W91 to V162C−CPM distance for the open subunit interface is therefore 35 Å, in strong agreement with the value determined for A42C/V162C/W198F/A213C. Opening of one subunit interface (the second model) is much more likely to be accommodated by gp45 than the gross structural changes at all three subunit interfaces required by the first model.

Having demonstrated a 35−38 Å solution distance between W91 and V162C−CPM, consistent with one open subunit interface in the gp45 trimer, we sought to construct models of gp45 that take into account this distance as well as to use the loop region as a pivot point for converting the X-ray crystal structure into a putative open complex. Figure 6 shows the top and side views of two models, one that opens the complex within the plane of the torus (part B) and a second that opens the complex out of the plane of the torus (part C), with the W91−V162 Cα−Cα distance increasing from 14 Å found in the X-ray crystal structure to 38 Å found by fluorescence. The closest amino acid side chains across the opened subunit interface are separated now by 28 and 13 Å for the in-plane and out-of-plane models, respectively. The diameter of DNA is about 25 Å, making the separation between the two subunits in the in-plane model just sufficient to allow DNA to pass into the center of the ring.

Interestingly, it has been previously shown that a large excess of gp45 over gp43 in the presence of the macromolecular crowding agent poly(ethylene glycol) can be used to form the holoenzyme in small quantities without gp44/62. Using these conditions, the holoenzyme could even be assembled onto primed, single-stranded circular M13 DNA (*46*), suggesting that gp45 loading was occurring through an open trimer rather than threading the end of the DNA through a closed trimer. Macromolecular crowding strengthens heteroassociations to a much greater extent than it influences the position of a simple conformational equilibrium (such as between an open and closed trimer) (*47*, *48*). This would tend to drive the assembly of gp45 and gp43 onto DNA without forcing free gp45 into a closed trimer that would be unavailable for loading, although such an uncatalyzed process would still be much less efficient than with catalytic loading by gp44/62. Macromolecular crowding also strengthens self-associations (*47*, *48*), further depleting the concentration of gp45 monomers that would be available to form the holoenzyme in a very unlikely pentamolecular assembly process directly from gp45 monomers.

The above-described changes to make the in-plane and out-of-plane models were accomplished by altering the dihedral angle (28 and 29° for the in-plane and out-of-plane models, respectively; see Materials and Methods) of one backbone bond in the loop to cause the desired structural change. These structures do not necessarily represent an allowed conformation of the bond nor an energy-minimized structure. These two operations represent two pathways to

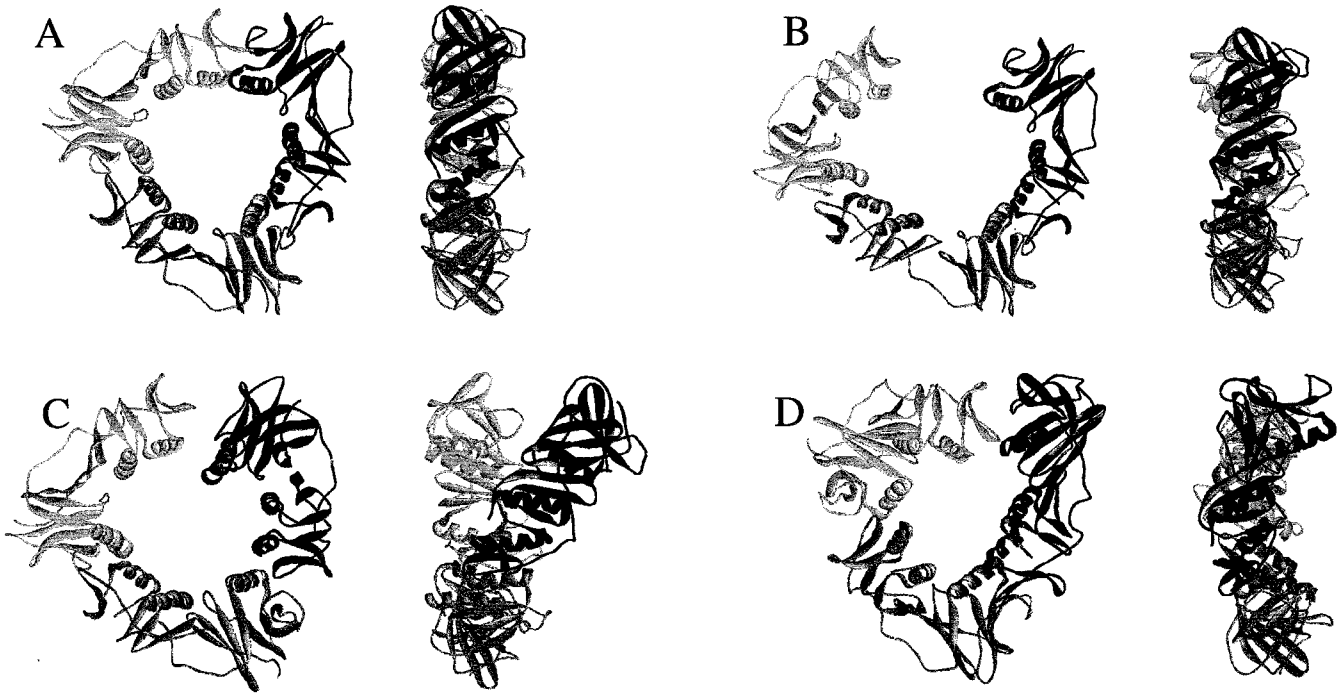

FIGURE 6: Top and side views of (A) the X-ray crystal structure, (B) the in-plane model, (C) the out-of-plane model, and (D) the puckered model of gp45.

open the closed, trimeric structure, but other pathways are not precluded. Likewise, other open structures consistent with the FRET data are not precluded.

These new solution structures along with the X-ray structure were used to calculate hydrodynamic parameters, which were then compared to the hydrodynamic parameters determined by velocity sedimentation. The program AtoB (*33*) was used to form a collection of about 560 spherical beads to represent the full structure (containing over 5000 atoms). These beads were used as input for the program HYDRO (*34*), developed for the prediction of sedimentation coefficients as well as other hydrodynamic parameters. The structure solved by X-ray crystallography, which represents the closed form of the complex, gave an estimated sedimentation coefficient of 4.72 S, while the in-plane and out-of-plane models gave 4.48 and 4.77 S, respectively. From a qualitative standpoint, only the in-plane model is consistent with our observations (a decrease in sedimentation coefficient moving from a closed to an open complex). The out-of-plane model actually appears to make the complex more symmetric or spherical as evidenced by the slight increase in estimated sedimentation coefficient.

The sedimentation coefficients estimated by HYDRO can be corrected for protein hydration using eq 8 (*36*). AtoB gave a hydration estimate of 0.36 g/g for gp45 from the amino acid content (*35*). Equation 8 yields 4.14, 3.93, and 4.19 S for the X-ray crystal structure, the in-plane model, and the out-of-plane model, respectively, for a hydration of 0.36 g/g. Hydration estimates from the amino acid content tend to be slightly higher than the experimental value since water is often excluded from the inside of proteins (*35*). A small decrease in the hydration estimate would cause a slight increase in the corrected sedimentation coefficients. The corrected sedimentation coefficient from HYDRO for the in-plane model therefore has the best match for the experimental sedimentation coefficient of wild-type gp45 (3.93 versus 4.0 S, respectively).

There is not a match between these three predicted sedimentation coefficients and the experimental sedimentation coefficient for cross-linked A42C/A213C, which therefore necessitates a more spherical or symmetric model. The X-ray crystal structure was altered to cause the ring to pucker out of the plane (see Figure 6D), requiring the alteration of three dihedral angles but maintaining the W91−V162C distance found in the X-ray crystal structure. This structure yielded a sedimentation coefficient of 5.33 S as predicted by HYDRO, which was corrected to 4.68 S by eq 8. This value is a good match for the experimental sedimentation coefficient of cross-linked A42C/A213C and qualitatively suggests a structure more consistent with the solution structure of cross-linked A42C/A213C than the X-ray crystal structure. For cross-linked R87C/T167C and the loop mutants P105G and P107G, solution structures lying between the X-ray crystal structure and the puckered model would be most consistent with the intermediate $S^{\circ}_{20,w}$ values found for these mutants.

Using this additional evidence, we propose that wild-type gp45 exists in solution as an open complex, with 38 Å separating the open interface, and this opening occurs within the plane of the ring. Because of the small number of solution constraints available to us at this time and, therefore, the qualitative nature of the present solution structure of wild-type gp45, experiments to refine this solution structure further using additional FRET pairs are currently underway. In addition, these FRET experiments will be able to distinguish between the in-plane and out-of-plane models for wild-type gp45 interacting with gp44/62 before and after loading onto DNA, as well as determine the direction and magnitude of these conformational changes.

Our conclusion that gp45 exists as an open trimer in solution is not necessarily at odds with the closed trimer that was observed by X-ray crystallography. We speculate that gp45 may be in equilibrium between an open and closed form, with the compact and 3-fold symmetric closed form

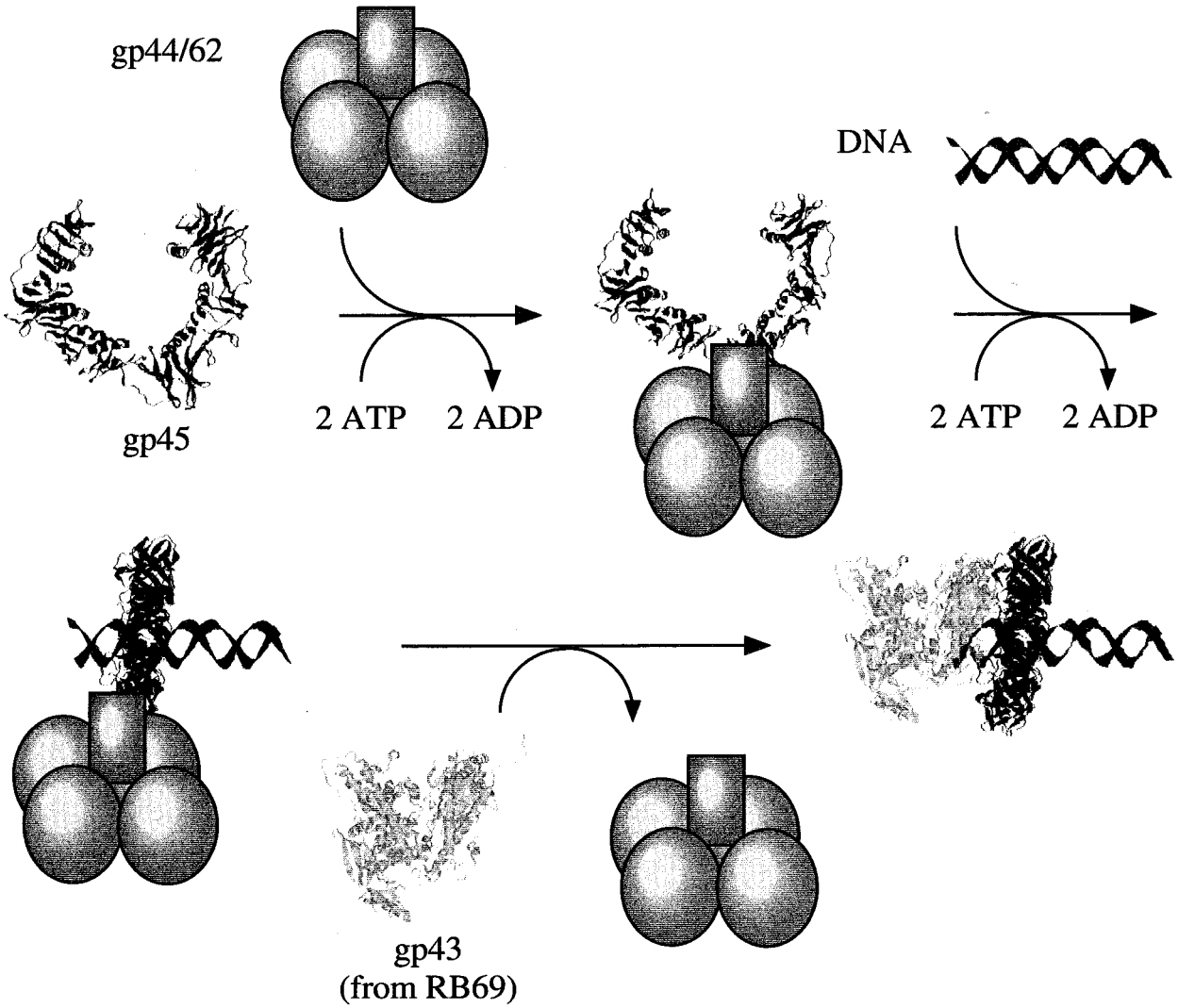

FIGURE 7: Proposed mechanism of holoenzyme assembly.

more likely to crystallize than the open form. Since our steady-state fluorescence measurements observe the average solution conformation of an ensemble of gp45 molecules, our results would also be consistent with a mixed population of open and closed trimers. We are currently using time-resolved fluorescence measurements to determine if such an equilibrium exists and to measure the equilibrium constant. For A42C/V162C/W198F/A213C, the upper limit for the population of closed trimers is 22% [$E_u = (2E_c + (\%\ \text{open})\text{-}E_o + (\%\ \text{closed})E_c)/3$], assuming a transfer efficiency of zero (and a W91 to V162C−CPM distance greater than 60 Å) for the open interface.

Figure 7 shows a model for the assembly of the holoenzyme onto DNA taking into account previous results as well as those presented here. Starting from gp45 open in solution, gp44/62 binds and induces a conformational change in gp45 that allows DNA to pass into the center of the ring. This process requires the hydrolysis of two molecules of ATP (*42*) and may be the conformational change observed by fluorescence and photo-cross-linking (*8*−*10*). At this time, we cannot determine the direction (in-plane versus out-of-plane or other) and magnitude of this motion.

The model in Figure 7 shows that gp44/62 binds gp45 predominantly on one subunit of gp45 centered at the proline-rich loop to allow free passage of DNA into the central hole through the opposing and opened subunit interface. Gp44/62 interacts with the same face of gp45 as gp43 (*49*), but potentially at distinct locations on gp45. Upon interaction with DNA, gp45 is closed by gp44/62 onto the DNA concomitant with hydrolysis of the final two ATP molecules (*42*). This second conformational change has also been observed previously (*8*−*10*). Finally, gp43 can bind to gp45 through the agency of gp44/62 and complete, upon the loss of gp44/62, the assembly of the holoenzyme. No further conformational changes were observed in gp45 upon binding of gp43 (*8*), suggesting that the final conformational change induced by gp44/62 places gp45 in the conformation found in the holoenzyme.

Modeling the RB69 DNA polymerase X-ray crystal structure (*7*) with the gp45 X-ray crystal structure shows that gp43 can contact predominantly two subunits of gp45 when docked together. It has been observed that the rate of gp45 subunit exchange drops to one-third that of free gp45 when in a holoenzyme complex bound to DNA (*11*). One may infer that two of the three subunits of gp45 are prevented from dissociating by gp43, and the rate of subunit exchange is dictated by release of the third, unbound subunit. We have threaded the C-terminal tail of gp43 into one of the interfaces

between gp45 subunits. This interface would be the one opening and closing if gp44/62 binding and gp45 motion is centered on the opposing loop of gp45. This would provide a stronger linkage between gp43 and gp45 and is consistent with the observation that the C-terminal tail of gp43 is absolutely required for formation of the holoenzyme (*50*).

In conclusion, we have used the combination of analytical ultracentrifugation, fluorescence, and hydrodynamic modeling to show that bacteriophage T4 gp45 forms an open, trimeric complex in solution. These results further clarify the model of holoenzyme assembly, although detailed structures of the holoenzyme and its intermediate forms during assembly remain yet to be elucidated. The use of FRET to measure the distance across the open gp45 subunit interface should prove to be valuable in determining the conformation of gp45 during and after assembly of the holoenzyme onto DNA, providing additional structural and mechanistic information.

ACKNOWLEDGMENT

We thank Ismail Moarefi and John Kuriyan for providing the X-ray structure coordinates of gp45 before publication, as well as Borries Demeler, William Cannon, Tracy Nixon, and Olwyn Byron for helpful discussions.

REFERENCES

1. Kong, X.-P., Onrust, R., O'Donnell, M., and Kuriyan, J. (1992) *Cell 69*, 425−437.
2. Krishna, T. S. R., Kong, X.-P., Gary, S., Burgers, P. M., and Kuriyan, J. (1994) *Cell 79*, 1233−1243.
3. Kuriyan, J., and O'Donnell, M. (1993) *J. Mol. Biol. 234*, 915−925.
4. Stillman, B. (1994) *Cell 78*, 725−728.
5. Kaboord, B. F., and Benkovic, S. J. (1995) *Curr. Biol. 5*, 149−157.
6. Wang, C.-C., Yeh, L. S., and Karam, J. D. (1995) *J. Biol. Chem. 270*, 26558−26564.
7. Wang, J., Sattar, A. K. M. A., Wang, C.-C., Karam, J. D., Konigsberg, W. H., and Steitz, T. A. (1997) *Cell 89*, 1087−1099.
8. Sexton, D. J., Carver, T. E., Berdis, A. J., and Benkovic, S. J. (1996) *J. Biol. Chem. 271*, 28045−28051.
9. Latham, G. J., Pietroni, P., Dong, F., Young, M. C., and von Hippel, P. H. (1996) *J. Mol. Biol. 264*, 426−439.
10. Pietroni, P., Young, M. C., Latham, G. J., and von Hippel, P. H. (1997) *J. Biol. Chem. 272*, 31666−31676.
11. Soumillion, P., Sexton, D. J., and Benkovic, S. J. (1998) *Biochemistry 37*, 1819−1827.
12. Jarvis, T. C., Paul, L. S., and von Hippel, P. H. (1989) *J. Biol. Chem. 264*, 12709−12716.
13. Maniatis, T., Fritsch, E. F., and Sambrook, J. (1989) *Molecular Cloning: A Laboratory Manual*, Cold Spring Harbor Laboratory, Plainview, NY.
14. Barik, S. (1993) *Methods Mol. Biol. 15*, 277−286.
15. Nossal, N. G. (1979) *J. Biol. Chem. 254*, 6026−6031.
16. Rush, J., Lin, T.-C., Quinones, M., Spicer, E. K., Douglas, I., Williams, K. R., and Konigsberg, W. H. (1989) *J. Biol. Chem. 264*, 10943−10953.
17. Frey, M. W., Nossal, N. G., Capson, T. L., and Benkovic, S. J. (1993) *Proc. Natl. Acad. Sci. U.S.A. 90*, 2579−2583.
18. Ellman, G. L. (1958) *Arch. Biochem. Biophys. 74*, 443−450.
19. Berdis, A. J., and Benkovic, S. J. (1996) *Biochemistry 35*, 9253−9265.
20. Kaboord, B. F., and Benkovic, S. J. (1996) *Biochemistry 35*, 1084−1092.
21. Johnson, M. L., Correia, J. J., Yphantis, D. A., and Halvorson, H. R. (1981) *Biophys. J. 36*, 575−588.
22. Schachman, H. K. (1959) *Ultracentrifugation in Biochemistry*, Academic Press, New York.
23. Goldberg, R. J. (1953) *J. Phys. Chem. 57*, 194−202.
24. van Holde, K. E., and Weischet, W. (1978) *Biopolymers 17*, 1387−1403.
25. Cantor, C. R., and Schimmel, P. R. (1980) *Biophysical Chemistry, Part II*, Freeman, San Francisco.
26. Stryer, L. (1978) *Annu. Rev. Biochem. 47*, 819−846.
27. Jezewska, M. J., Rajendran, S., and Bujalowski, W. (1998) *J. Biol. Chem. 273*, 9058−9069.
28. Epps, D. E., Poorman, R., Hui, J., Carlson, W., and Heinrikson, J. (1987) *J. Biol. Chem. 262*, 10570−10573.
29. Chabbert, M., Lukas, T. J., Watterson, D. M., Axelson, P. H., and Prendergast, F. G. (1991) *Biochemistry 30*, 7615−7630.
30. Selvin, P. R. (1995) *Methods Enzymol. 246*, 300−334.
31. Hass, E., Katchalski-Katzir, E., and Steinberg, I. Z. (1978) *Biochemistry 17*, 5064−5070.
32. Efnik, M. R. (1991) in *Topics in Fluorescence Spectroscopy Volume 2* (Lakowicz, J. R., Ed.) pp 53−120, Plenum Press, New York.
33. Byron, O. (1997) *Biophys J. 72*, 408−415.
34. Garcia de le Torre, J., Navarro, S., Lopez Martinez, M. C., Diaz, F. G., and Lopez Cascales, J. J. (1994) *Biophys. J. 67*, 530−531.
35. Kuntz, I. D., and Kauzmann, W. (1974) *Adv. Protein Chem. 28*, 239−345.
36. Squire, P. G., and Himmel, M. E. (1979) *Arch. Biochem. Biophys. 196*, 165−177.
37. Demeler, B., Saber, H., and Hansen, J. C. (1997) *Biophys. J. 72*, 397−407.
38. Lillo, M. P., Beechem, J. M., Spikowska, B. K., Sherman, M. A., and Mas, T. M. (1997) *Biochemistry 36*, 11261−11272.
39. Wu, P., and Brand, L. (1994) *Anal. Biochem. 218*, 1−13.
40. van der Meer, B. W., Coker, G., and Chen, S.-Y. S. (1994) *Resonance Energy Transfer Theory and Data*, VCH, New York.
41. Dunn, B. M., Pham, C., Raney, L., Abayasekara, D., Gillespie, W., and Hsu, A. (1981) *Biochemistry 20*, 7206−7211.
42. Sexton, D. J., Kaboord, B. F., Berdis, A. J., Carver, T. C., and Benkovic, S. J. (1998) *Biochemistry 37*, 7749−7756.
43. Yao, N., Turner, J., Kelman, Z., Stukenberg, P. T., Pan, Z.-Q., Hurwitz, J., and O'Donnell, M. (1996) *Genes Cells 1*, 101−113.
44. Demeler, B., and Saber, H. (1998) *Biophys. J. 74*, 444−454.
45. Lakowicz, J. R. (1983) *Principles of Fluorescence Spectroscopy*, Plenum Press, New York.
46. Reddy, M. K., Weitzel, S. E., and von Hippel, P. H. (1993) *Proc. Natl. Acad. Sci. U.S.A. 90*, 3211−3215.
47. Minton, A. P. (1981) *Biopolymers 20*, 2093−2120.
48. Minton, A. P. (1983) *Mol. Cell. Biochem. 55*, 119−140.
49. Latham, G. J., Bacheller, D. J., Pietroni, P., and von Hippel, P. H. (1997) *J. Biol. Chem. 272*, 31685−31692.
50. Berdis, A. J., Soumillion, P., and Benkovic, S. J. (1996) *Proc. Natl. Acad. Sci. U.S.A. 93*, 12822−12827.

BI9827971